Tanzania Journal of Science 49(5): 1151-1163, 2023
ISSN 0856-1761, e-ISSN 2507-7961
© College of Natural and Applied Sciences, University of Dar es Salaam, 2023

Micro Machining of a Si_3N_4/SiO_2/Ti/Pt Hotplate and Its IR Emissivity Properties

Egidius R. Rwenyagila
Physics Department, University of Dar es Salaam, P. O. Box 35063, Dar es Salaam, Tanzania.
Corresponding email: egidiusrrwenyagila@gmail.com
Received 4 Aug 2023, Revised 2 Nov 2023, Accepted Dec, Published Jan 2024
https://dx.doi.org/10.4314/tjs.v49i5.17

Abstract

This paper presents the fabrication processes for a Si_3N_4/SiO_2/Ti/Pt membrane based micro hotplate (MHP) using photolithography (PL) micro-machining techniques. The properties of the MHP filament are investigated and overall performance characteristics with regard to infrared (IR) radiation emissivity, resistance, breakdown voltage, and temperature of the fabricated Si_3N_4/SiO_2/Ti/Pt micro heater. During characterization, the results show the device breakdown voltage of 24.24 V corresponding to the optimum operation temperature of ~ 1730.30 K. The device also showed an emissivity value of 5.2% with ~ 7% efficiency of transforming electrical power to IR thermal radiation power. The relationship between temperature and resistance, behaviour of fourth power of temperature and thermal response time constant of IR radiation obtained from direct experimental measurements, analytical calculations and extrapolations are shown to provide practical parameters that are needed for applications of MHP in IR radiation sources.

Keywords: IR Emissivity, micro-hotplate, photolithography, platinum

Introduction

Micro-machined devices, such as platinum (Pt) micro-hotplates (MHPs) are of great interest (Samaeifar et al. 2015, Shwetha and Rudraswamy 2021) primarily due to their low power consumption (Liu et al. 2018), quick thermal response time (Prasad et al. 2015) and low cost (Li et al. 2021, Yuan et al. 2022). This makes microhotplates useful for applications in different types of micro-electro-mechanical-system (MEMS) technologies (Courbat et al. 2008, Liu et al. 2018). Due to miniature resistive nature (Liu et al. 2018), MHPs are also known to exhibit high-temperature over an active heating zone while the rest of the device remains at surrounding temperature (Kalinin et al. 2021). Consequently, MHPs are widely used in flow sensors (Bose et al. 1998), actuators and micro-heaters (Sarro et al. 1994), gas sensors (Simon et al. 2001, Zhou and Zhang 2021), micro-thrusters (Rossi et al. 2006), and IR radiation sources (Konz et al. 2005, Liu et al. 2018) for use in security alarms and other automated technologies. The MHPs are produced generally by photolithography (PL) micro-machining techniques using pre-patterned masks such as those made of transparent quartz with highly absorbing chromium on top of photoresists (PRs) (Simon et al. 2001, Baroncini et al. 2004, Courbat et al. 2008, Kalinin et al. 2021).

The performance properties such as power consumption, maximum operating temperature, mechanical and other MEMS properties of MHPs are known to depend on the device dimensions, electrical and thermal properties of the MHP materials (Prasad et al. 2015). The potential MHP heating element resistive material candidates include platinum (Pt) (Briand et al. 2002), polysilicon (poly-Si) (Afridi et al. 2002), nickel (Ni) (Yan et al. 2008), tungsten (W) (Ali et al. 2008) and gold/titanium (Au/Ti) (Zhang et al. 2007) thin

films. However, gold in Au/Ti was reported to have drawbacks of low resistivity and poor adhesion (Puigcorbe et al. 2003), similar for Al with low resistivity, poor adhesion and electro-migration (Simon et al. 2001). Furthermore, Al (Simon et al. 2001) and Ni (Marciuš et al. 2012) are known to oxidize easily at temperatures between ∼400 and 800°C. Similar oxidation cases have been reported for W with disadvantage of forming oxide at temperatures higher than 1200°C, therefore, expensive vacuum conditions are usually required for W at these temperatures (Prasad et al. 2015). Poly-Si suffers from drift of temperature coefficient of resistance (TCR) at higher operating temperature and is easily attacked by Si etching solutions such as tetramethylammonium hydroxide (TMAH) and potassium hydroxide (KOH) during bulk micromachining process (Afridi et al. 2002, Prasad et al. 2015).

Consequently, earlier reports referring to MHPs (Guidi et al. 1998, Briand et al. 2003) have suggested use of functional thin films of Pt (Prasad et al. 2015) sputtered on an n-type (100) Si wafers (Mo et al. 2001) as an ideal candidate material for MHP applications (Schössler et al. 2020), because of highly stable TCR and chemical stability of Pt (Courbat et al. 2008). Furthermore, Pt has the attractive combinations of promising practical properties that include chemical inertness, thermal stability, oxidation and corrosion resistance, high ductility, and relatively high melting temperature of up to > 2000 K at ambient pressure (Prasad et al. 2015). Also, Pt has the advantages of reliability and reproducibility that enable it to sustain large current densities and high operation temperature without structural damage (Prasad et al. 2015).

However, despite the promising practical properties and the widespread interest in Pt based MHPs in recent years, most of the literature on Pt based micro-heaters are mainly focused on the stability and reliability of the devices such as thermal mechanical behaviours (Firebaugh et al. 1998, Briand et al. 2005, Courbat et al. 2008). Noteworthy however that, the electrical and thermal properties such as IR emissivity of micro-machined structures are very important parameters since they define fundamental practical variables that are needed for operation of MHP devices at optimal efficient performances (Cardinali et al. 1997, Faglia et al. 1999, Baroncini et al. 2004). Furthermore, two techniques, namely, closed-membrane and suspended-membrane have been proposed for the stacking of PL machined micro-device structures and components (French et al. 1997, Simon et al. 2001, Mo et al. 2001, Liu et al. 2018). Although, not reported by many authors, membrane fabrications of the micro-machined devices are known to be a critical step that attracts significant research interest in sensor development technology (Puigcorbe et al. 2003, Zhang et al. 2008).

The IR emissivity behaviour of structured Pt MHPs and their applications, particularly in technologies requiring efficient transformation of electrical power to thermal radiation power are also critical challenges demanding for research solutions and they are rarely reported in literature (Mo et al. 2001). Thus, investigation of the fabrication processes of Pt based MHPs for IR radiation source applications are significant steps in micro structuration for sensor research and development. This paper reports a step by step structuration and characterization of a Si_3N_4/SiO_2/Ti/Pt micro-heater using PL process. The electrical and IR emissivity behaviour of the obtained Pt MHP sample are also measured and analysed for efficient transformation of electrical power to thermal radiation power, relationship between temperature and resistance, behaviour of 4^{th} power of temperature and thermal response time constant.

Materials and Methods

Photolithography technique

The contemporary PL technique was reported earlier in literature (Briand et al. 2000). Using similar PL procedure, the device patterns on the pre-fabricated mask were systematically transferred onto an n-type (100) Si wafer to produce desirable MHP geometries. Device fabrication processes involved selective exposure to a ultra-violet (UV) light radiation source using a positive

photoresist (PPR) made of diazonaphtoquinone in Novolac (Guidi et al. 1998). Prior to the development stage, the PPR was illuminated with UV light using a solar spectra simulator. The illumination was followed by development of the PPR using aqueous KOH alkaline solution at a temperature between 80–120 ^{o}C, similar temperature range were used in earlier investigations (Guidi et al. 1998, Briand et al. 2000, Mo et al. 2001).

The closed-membrane method with Si_3N_4/SiO_2 layers stacked on Si wafer was used for embedding of Ti/Pt MHP wires. In this method, MHP stacked with appropriate Si_3N_4/SiO_2 membrane materials were patterned via anisotropic etching of bulk Si from the backside (Mo et al. 2001). Wet etching method was used because it is cost effective. The potentially useful wet etchants are KOH, TMAH and ethylene diamine pyrocatechol (EDP) (French et al. 1997, Briand et al. 2000, Simon et al. 2001, Mo et al. 2001, Courbat et al. 2008). However, TMAH is toxic, while KOH and EDP are both safe, the latter is avoided because is expensive, therefore, the most favourable option etchant, KOH was used in the current work. Silicon nitride (Si_3N_4) and silicon oxide (SiO_2) were used to stop etching of undesired regions during wet etching with KOH (Simon et al. 2001). SiO_2 and Si_3N_4 were selected because of their low thermal conductivities that provide good thermal isolation between the heated active zone and the membrane rim (Simon et al. 2001).

After achieving desirable MHP geometries using PPR, dry etching of Pt, Si_3N_4 and SiO_2 were achieved using chlorine (Cl_2), hexafluoroethane (C_2F_6) and octafluorocyclobutane (C_4F_8), respectively. The bulk micromachining involved anisotropic orientation dependent wet etching of Si from the backside of the wafer. This required the edges of the mask patterns to be aligned along the directions comprising the (111) planes. As shown in Figure 1, because of anisotropy, the etch rate of Si (111) surface is usually slower than that of the Si (100) surface. This resulted to selective etching towards the Si (111) plane and determined the shape of the sidewalls since Si (100) wafer was used as starting substrates similar to earlier work (French et al. 1997, Briand et al. 2000). An excellent contemporary physics of the various mechanisms during fabrication of an etched profile of controlled dimensions are reported elsewhere (Purohit et al. 2022).

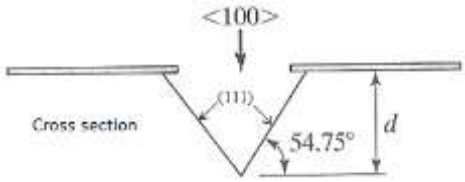

Figure 1*:* Schematic illustration of anisotropic etching of Si (100) wafer

Microhotplate sample

Preparation of the MHP sample involved use of 20 nm titanium (Ti) as an adhesion layer as proposed by Schössler et al. (2020) to deposit a 100 nm Pt film on $Si/SiO_2/Si_2N_4$ wafer substrate by DC sputtering. Figure 2 shows schematic representation of the different thin layers that were deposited on the substrate along with their corresponding thicknesses. The different films of varying thicknesses, other than Ti and Pt films were added to improve robustness and protection of the micro-heater (Briand et al. 2000). The respective layers of SiO_2 and Si_3N_4 were prepared by conventional techniques of thermal oxidation and low pressure chemical vapour deposition. Materials growth approaches used in this work were similar to those used in previous investigations for SiO_2 (Fogarassy et al. 1987, Deal and Grove 1965) and Si_3N_4 (Cossou et al. 2019).

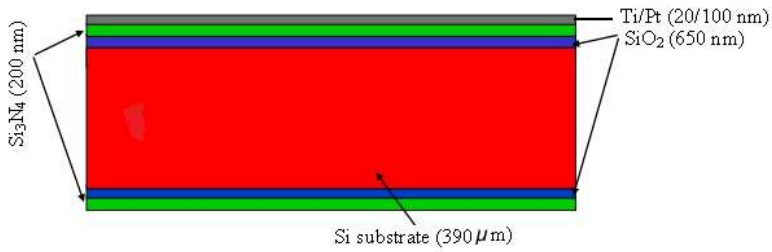

Figure 2*:* Schematic illustration of the different thin film layers and thicknesses of materials deposited on Si (100) wafer before patterning of micro-hotplate

Then, starting with the material thin film layers on the substrate (Figure 2), the standard PL process was undertaken. To finish the PL process, substrate control protocol was carried out using an optical microscope to test the effectiveness of the machining steps and the geometry of the patterned materials. Lastly, the filament wires were made by etching the Pt with Cl_2, followed by striping of the PPR using oxygen plasma set to a potential difference of 500 V. After etching of Pt, a SiO_2 passivation membrane layer was deposited and etched to protect the micro-structured Pt wires to prevent them from leaking the current during characterization. To establish the etching characteristics for SiO_2 passivation layer on top of the Pt micro-wires, firstly, a layer of a PPR was spin coated, followed by exposure after mask and wafer alignment before development and stripping to remove unprotected soluble parts of the PPR. The etching of SiO_2 was achieved at a rate of 80 nm per minute for the duration of 3 minutes using a buffered hydrogen fluoride (BHF) at room temperature (25 °C). After etching of SiO_2, the wafer was rinsed in deionised water for few minutes followed by after etch resistance inspection with a resistance meter before drying in a rotor machine. During ultra-cleaning, the resistance meter went up to 12.40 $M\Omega$ signifying that the substrate was well cleaned. Finally, the PPR was removed by stripping using oxygen plasma machine set at 500 V.

Backside bulk micromachining

In order to protect the backside of the wafer during Si etching, a PPR (AZ ECI 3027, Microchemicals GmbH, Germany) was coated on the backside of the wafer, using a coater machine (Ritetrack 88, CAE CA, USA) followed by baking on 115 °C hotplate for 1 minute and cooled to room temperature. The cooled wafer was aligned with a mask and exposed to the UV light at a rate of 10 $mWcm^{-2}$ for 9.5 sec on the mask aligner machine. Lastly, the exposed PPR was developed to remove the soluble parts and establish the necessary conditions for Si_3N_4 and SiO_2 etching process. The unprotected regions of Si_3N_4 were first removed by dry etching at a rate of 0.26 µm per minute during a 1-minute time using C_2F_6 followed by two minutes etching of SiO_2 at a rate of 0.34 µm per minute with C_4F_8. After removal of Si_3N_4 and SiO_2, an unexposed layer of the PPR was removed by dry stripping using plasma oxygen in a plasma striper machine (Tepla 300, Milano, Italy).

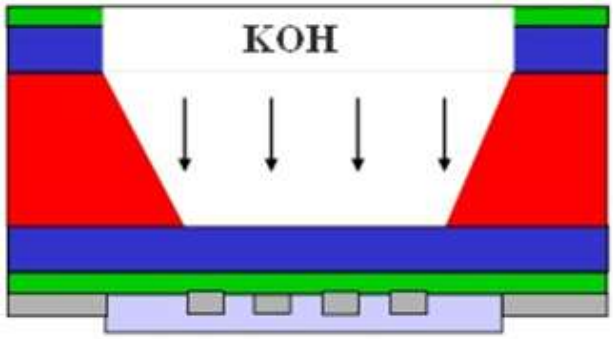

Figure 3*:* Schematic of the MHP patterns after backside bulk micromachining of the Si wafer

For the anisotropic etching of Si window, first, the wafer was prepared by fixing it in a thorough cleaned chuck, followed by Si wet etching by dipping the wafer on the chuck in a 40% KOH bath, a concentration that was used earlier by Briand et al. (2000). After Si etching process had started as indicated by bubbles coming out of the bath, the process was left to run overnight for 26 hours. After which neutralization and backend processes were undertaken to make a complete Pt based MHP device with dimensions shown in Figure 4.

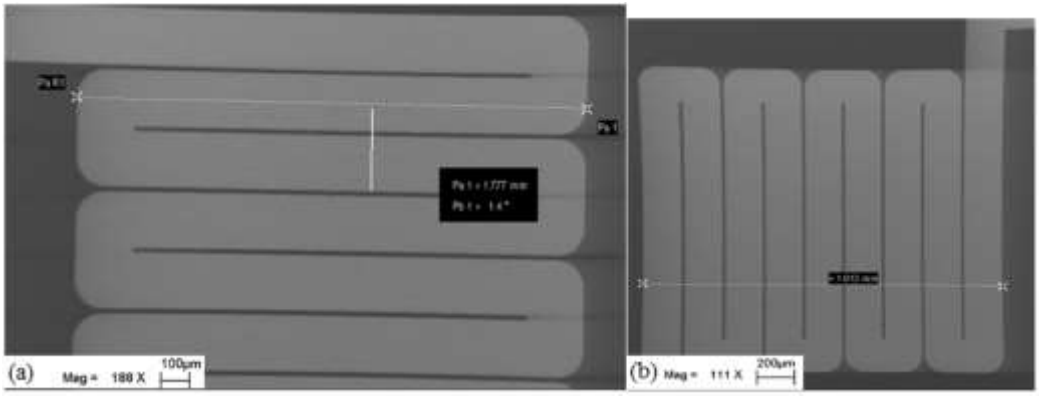

Figure 4*:* Optical picture illustrating dimensions of (a) length and (b) width of the PL structured Ti/Pt MHP filament coil

Sample characterization

The resistance-temperature relationship of metal materials such as Pt with constant TCR independent of temperature is described by the first-order function. This is given by equation 1 (Mo et al. 2001, Baroncini et al. 2004):

$$TCR = \frac{R_T - R_0}{R_0(T - T_0)} \qquad 1$$

where R_T is the resistance at temperature T and R_0 is resistance at room temperature (25 ^oC).

The TCR of Pt/Ti based thin films has been shown to range between 0.002 K^{-1} (Briand et al. 2000) and 0.0024 K^{-1} (Mo et al. 2001). The standard value of Pt filament resistance is also reported to range between 150–190 Ω at room temperature (Briand et al. 2000). However, in the current work, the values of TCR and room temperature resistance of the Ti/Pt MHP device sample measured directly with a voltmeter were found to be $1.4 \times 10^{-3}\ K^{-1}$ and 243.74 Ω, respectively. The discrepancies between the TCR and resistance values from this work and those reported in literature can be attributed to various factors. These may include changes in materials properties as a result of experimental procedure along with influences of SiO_2 and Si_3N_4 layers in which the Pt/Ti wire was

embedded. Figure 5 presents the experimental setup for the measurement of thermal responses of the MHP driven by the square voltage from a function generator. The thermal responses were measured with a micro area IR sensor with setup parameters shown in the Table 1.

Table 1: Parameters for emissivity characterization of a micro-machined Pt hotplate

Parameter	Value
IR source – sensor distance, R	11 mm
Area of the IR source, A_{source}	4 mm^2
Area of the sensor, A_{sensor}	1 mm^2
Sensitivity of the sensor, S	0.22 V/W
Voltage gain/amplification factor	5×10^4

Within this thermal measurement setup range, the radiated power was detected by the IR sensor before being measured using an oscilloscope (Figure 5). Theoretically, the radiated power detected by the sensor is given by equation 2.

$$P_{sensor} = \frac{U_{oscilloscope}}{S} = \varepsilon\sigma T^4 A_{source}\left(\frac{A_{sensor}}{2\pi R^2}\right) \quad 2$$

where P_{sensor} is the radiation power detected by the sensor, ε is the emissivity (< 1), σ is Stefan constant ($5.67 \times 10^{-8} Wm^{-2}K^{-4}$) and T is the absolute temperature of the MHP IR source.

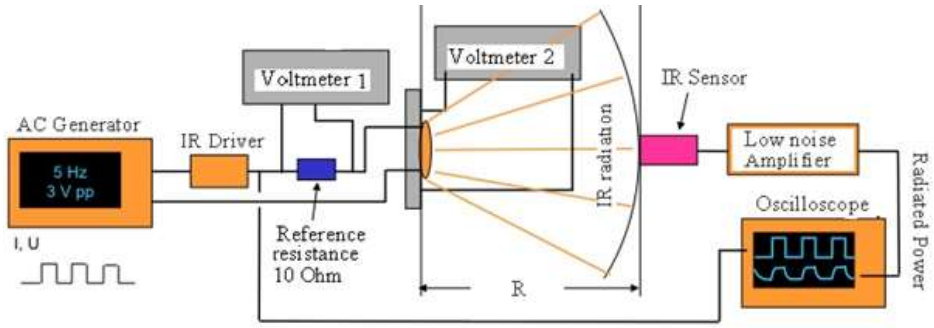

Figure 5 Experimental setup for characterization of emissivity of the Ti/Pt MHP sample

Results and Discussion

Figures 6 (a)–(d) present the values of the generator transient voltages that were applied and the corresponding voltages across the MHP IR source device (Figures 6 (a) and (b)) and those across the reference resistor (Figures 6 (c) and (d)) in accordance with the experimental setup shown in Figure 5. Notably, from Figure 6 the voltages across the 10 Ω reference resistor were negligibly small compared to the voltages across the MHP IR source. This is because the resistance of the Ti/Pt MHP filament is significantly larger than the 10 Ω reference resistance, since the reference resistor and the MHP device were connected in a series circuitry (Figure 5) to allow the same current to flow across them. With increasing voltage, the MHP IR source device was damaged at a value of 24.24V.

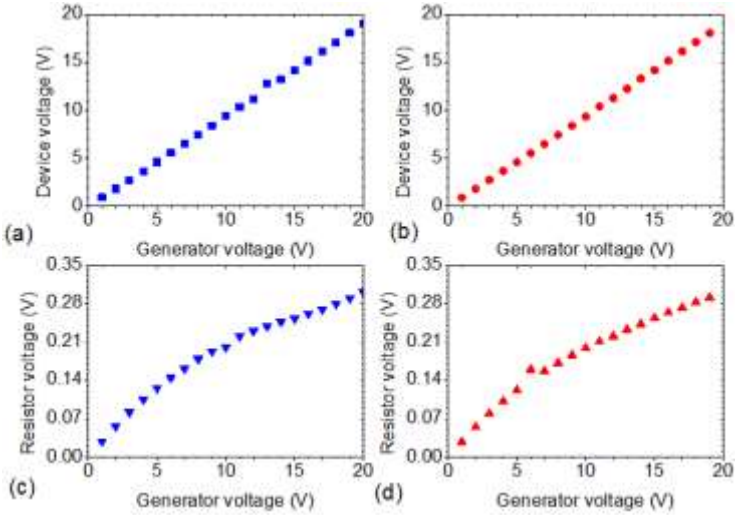

Figure 6*:* Functional generator – filament voltage relationship of a Pt MHP at voltages below breakdown limit for (a) forward and (b) backward device voltage measurements; (c) forward and (d) backward reference resistor voltage measurements

Thermal emission

The short-lived voltage response of a MHP IR source device driven by 15 V on the function generator and 14.2 V across the MHP device is presented in Figure 7. At this transient voltage response, the oscilloscope with an amplification factor of 5×10^4 recorded signal amplitude of 0.358 V as measure of the radiated power. Also, with the other voltages shown in Figure 6, the thermal response signals (not shown in this paper) showed similar emission response shapes with insignificant variations in signal amplitudes.

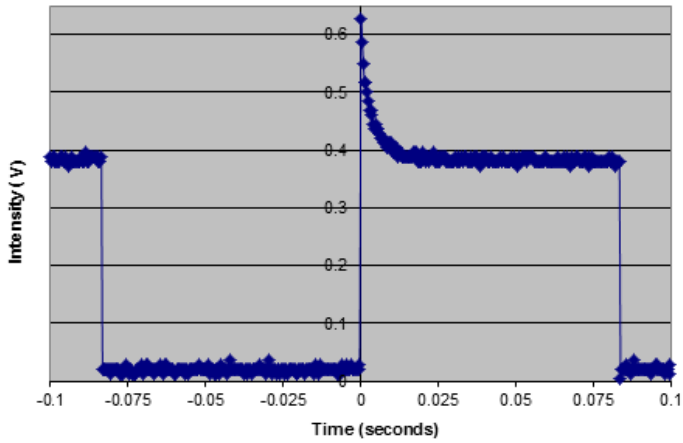

Figure 7*:* The transient voltage-time response illustrating the thermal emission of Pt MHP

Resistance-temperature properties

The reference resistor with a value of 10 Ω and the MHP device were purposely connected in series (Figure 5) with the voltage functional generator. This allowed same current, *I*, to flow through the resistor and the MHP sample device. As a result, the value of *I* is readily calculated from the well-known Ohm's law with respective resistance and voltage of 10 Ω and V_1 measure with first voltmeter 1 in Figure 5. This current is subsequently combined with the filament voltage V_2 measured with second voltmeter 2 in Figure 5 to obtain the filament resistance R_T

at any transient voltages below the MHP sample breakdown limit of 24.24 V.

The different values of R_T obtained at various MHP filament transient voltages were incorporated directly with the resistance-temperature analytical relationship (equation 1) in order to calculate the temperature of the MHP filament at particular instantaneous voltages. The resistance and temperature values at various MHP filament voltages were calculated using equations 3 and 4.

$$R_T = \frac{V_2}{I} = \frac{V_2}{V_1 \div R_0} \qquad 3$$

Combining equations 1 and 3 led to the expression for temperature values, T_i of the Pt MHP filament at given transient operation voltages given by equation 4.

$$T_i = \frac{R_T - R_0}{R_0 \times TCR} \qquad 4$$

where TCR and R_0 were directly measured and found to be 1.4×10^{-3} °C^{-1} and 243.74 Ω, respectively. The relationship between calculated temperature, voltage and resistance of the Pt MHP filament are presented in Figures 8 and 9. The temperature and resistance of the Pt MHP filament rise almost linearly with voltage with regression square value of 0.9937 for the case of temperature-voltage profile in Figure 8 and regression square value of exactly 1 for the temperature-resistance plot in Figure 9. This is attributed to the fact that as voltage increases, more electrical energy is converted to heat energy, hence the Pt MHP filament heats up. As a result of increasing temperature the resistance of the Pt MHP filament also rises (Figure 9).

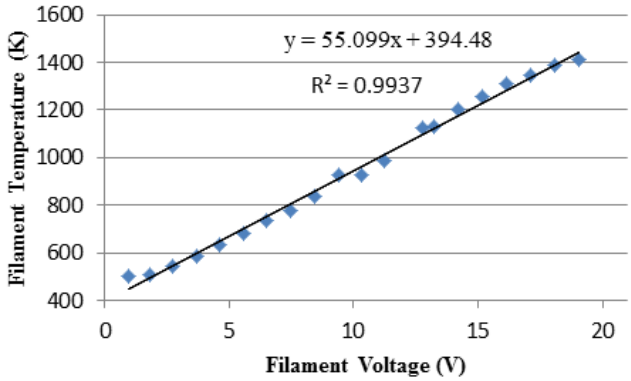

Figure 8*:* Temperature-voltage relationship for the Ti/Pt MHP filament sample

Figures 8 and 9 also revealed the typical characteristic advantages for most of resistance temperature detector (RTD) materials such as Pt. Thus, contrary to other group of materials such as negative temperature coefficient (NTC) thermistors, the RTD materials show linearly wide high temperature operating ranges. They also have better stability even at high temperatures. The extrapolation line of Figure 8 at the device breakdown voltage value of 24.24 V shows a temperature of 1730.30 K. Within possible acceptable experimental and environmental measurement artefactual errors, the device breakdown could be because in the proximity of the breakdown voltage the temperature of the device was close to the melting point of Pt.

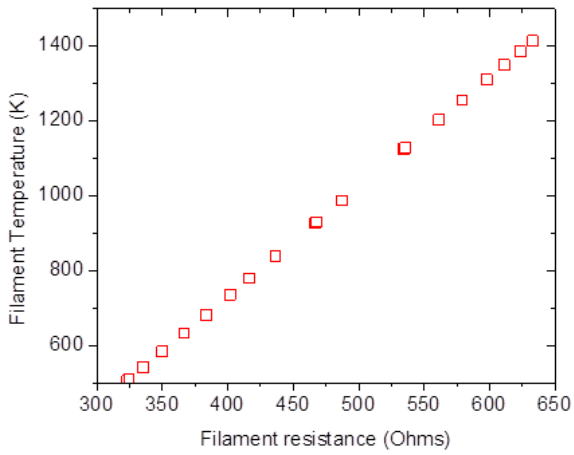

Figure 9*:* Linear temperature-resistance characteristics of fabricated Ti/Pt MHP filament

Effective fraction of radiation power

The Pt MHP IR source radiates energy in a spherical surface in space as shown in Figure 5. However, the absorbing surface area of the detecting IR sensor, projected within the MHP IR source direction is only a small part of the radiation sphere. This implies that the total power absorbed by the sensor was just a fraction of total power radiated from the IR source. The effective fraction, F of radiated power that was detected by the sensor can be estimated from the ratio of the total power absorbed by the sensor and the total power radiated by the radiation source. This is obtained from the ratio of the corresponding surface areas given by equation 5.

$$F = \frac{A_{sensor}}{2\pi R^2} \qquad 5$$

Since the area of the sensor used was 1 mm^2 and the distance between the Pt MHP IR source and the sensor, R was 11 mm (Table 1), the effective fraction of radiated power, F in percentage is about 0.13%.

Efficiency of transformation of electrical power

The efficiency, η of power transformation is obtained from the ratio of radiation power detected by the sensor and the input electrical power applied to the Pt MHP sample device. The detected radiation power is calculated from the effective power received by the sensor and the voltage sensitivity of the sensor shown in Table 1. The resulting value is normalized by dividing it to the effective fraction of the radiation received by the sensor. The electrical power applied to the Pt MHP device is obtained from the generalized Ohm's law as product of device voltage and current flowing through it at any transient point below breakdown voltage limit. The transient values, at which Figure 7 was recorded, with functional generator voltage of 15 V, Pt MHP filament voltage of 14.2 V and oscilloscope voltage of 0.358 V have been singled out and used in the calculation. In this case, the sensor voltage response and magnification values are given in Table 1. At this transient point the Pt MHP filament resistance was 561.26Ω. The power received by the sensor is therefore given by equation 6.

$$P_{sensor} = \frac{V_{oscilloscope}}{S} \qquad 6$$

With oscilloscope voltage of 0.358 V at an amplification factor of 5×10^4 and the sensor sensitivity factor of 0.22 VW^{-1}, the value of power received by the sensor was 3.25×10^{-5}W. This is divided to the effective fraction of radiated power, F to obtain the total power radiated from the Pt MHP IR source device. It is given by equation 7.

$$P_{radiated} = \frac{P_{sensor}}{F} \qquad 7$$

This gives the value of total radiated power of 2.5×10^{-2} W. The input electric power is obtained from equation 8.

$$P_{electric} = (IV)_{device} = \frac{V_{device}^2}{R_T} \qquad 8$$

At the device voltage of 14.4 V the resistance of the filament was 561.26 Ω, hence

resulting to total electric power of $3.6 \times 10^{-1} W$, with efficiency of transforming electric power to IR radiation of a Ti/Pt MHP now readily given by equation 9.

$$\eta_{transf} = \frac{P_{radiated}}{P_{electric}} \times 100\% \qquad 9$$

Thus, by inserting the values of radiated and electric power into equation 9 the efficiency of 6.94% of the Pt MHP transforming electric power to IR radiation is obtained.

Emissivity

The emissivity of the Pt MHP filament is calculated from the relation of the radiated power detected by the sensor. This is given by equation 10.

$$P_{sensor} = \frac{U_{oscillo}}{S} = \varepsilon \sigma A_{source} T^4 \left(\frac{A_{sensor}}{2\pi R^2}\right) \qquad (10a)$$

or equivalently by,

$$\varepsilon = \frac{2\pi R^2 P_{sensor}}{\sigma A_{source} T^4 A_{sensor}} \times 100\% \qquad (10b)$$

where $P_{sensor} = 3.25 \times 10^{-5} W$, $T = 1203.51\ K$, $\sigma = 5.67 \times 10^{-8}\ Wm^{-2}K^{-4}$ $A_{source} = 4\ mm^2$, $A_{sensor} = 1\ mm^2$, $R = 11\ mm$ (Table 1). Inserting these values into equation (10b), gives the Pt MHP IR emissivity value of ~ 5.2%.

Behavior of T^4

When a Ti/Pt MHP filament is heated by increasing the voltage, heat is created by the current flowing through it. This is according to Joule effect given by equation 11.

$$P = RI^2 \qquad 11$$

It is also true that IR emission intensity is proportional to the heat of the MHP filament. Since heat value increases with increasing resistance (Equation 11), the relationship between the filament resistance and the 4th power of temperature can provide realistic insights on the variation of radiated power with 4th power of the Pt MHP filament temperature. As shown in Figure 10, the 4th power of the MHP filament temperature increased significantly at low temperature values until a certain point where it started to show a slight increase as compared to low resistance region. This temperature-profile suggests that the corresponding rate of radiation increases with temperature until a certain saturation point in accordance with the radiation law. Accordingly, high temperature values result to high radiant energy intensity, I_r, in agreement with Stefan's statement given by equation 12.

$$I_r = \varepsilon \sigma A T^4 \qquad 12$$

where all the symbols takes their usual meaning.

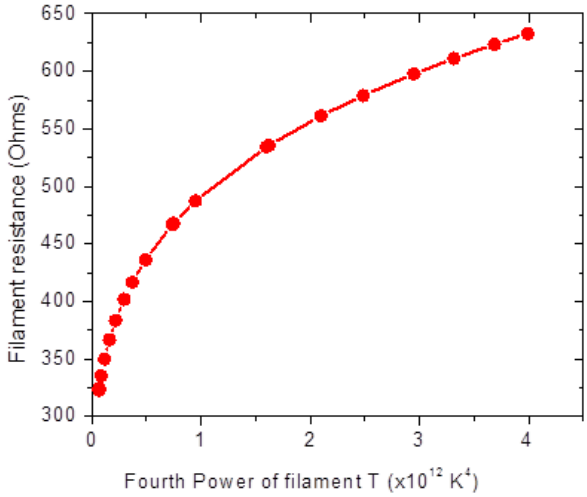

Figure 10*:* Relationship between MHP filament resistance and fourth power of temperature

Thermal response time constant

The thermal response time constant represents the amount of time required for the Pt MHP filament to reach 63.2% of its temperature difference when subjected to a step function change in temperature under negligible power dissipation conditions. The thermal response time constant can be estimated from analytical solution of Newton's law of cooling statement given by equation 13.

$$\frac{dT}{dt} = -\frac{\delta}{C}(T_i - T_0) \qquad 13$$

Generally equation 13 has a solution given by equation 14.

$$T = T_0 + (T_1 - T_0)exp\left\{-\frac{t}{\tau}\right\} \qquad 14$$

where T_i is the initial body temperature, t is time, C is heat capacity, δ is dissipation constant (the change in power dissipation per resulting filament temperature) and τ is the thermal time constant given by equation 15.

$$\tau = \frac{C}{\delta} \qquad 15$$

From the thermal emission data (Figure 7), direct analytical calculation of the thermal time constant is somewhat tedious. However, estimation of thermal properties including the thermal response time constant can be done via extrapolation based on the intensity response time and intensity amplitude dissipation shown by the device in Figures 7 and 11. As shown in the Figure 11, the time taken for the intensity to fall from ~ 0.64 to ~ 0.40 (63.2% of 0.64) is about 0.01 seconds. Ideally, this time gives the appropriate estimate value of the IR MHP thermal response time constant. Note however that, for fast response technologies, the value of 0.01 seconds is arguably a large time constant. The reason for this high response time constant could be attributed to the low sensitivity of the RTD materials that include Pt.

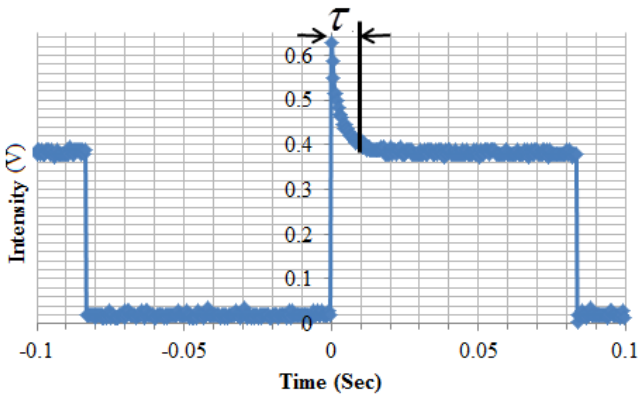

Figure 11: Illustration of thermal intensity time transient response and amplitude dissipation properties of the Ti/Pt MHP IR device

Conclusion

In this paper, a PL micro-machined Si_3N_4/SiO_2 membrane has been used to host a Ti/Pt MHP for IR emission purposes. The main characteristics features of the Pt MHP IR source have been established. Analytical calculation model of the thermal response behaviour of the MHP has been presented with accent to the IR emissivity properties. The results have highlighted interesting realistic IR emissivity properties for voltages below the breakdown limit of 24.24 V at a temperature of ~ 1730.30 K. The experimental TCR of the micro-structured Ti/Pt film was $1.4 \times 10^{-3}\ K^{-1}$ and thermal response time constant of about 0.01 s was found. The device also gave an emissivity value of 5.2% with ~ 7% efficiency of transforming electrical power to IR thermal radiation power.

Declaration of Competing Interest

The author declares no known conflict of interests in the work reported in this paper.

References

Afridi MY, Suehle JS, Zaghloul ME, Berning DW, Hefner AR, Cavicchi RE, Semancik S, Montgomery CB and Taylor CJ 2002 A monolithic CMOS microhotplate-based gas sensor system. *IEEE Sensors J.* 2(6): 644-655.

Ali SZ, Udrea F, Milne WI and Gardner JW 2008 Tungsten-based SOI microhotplates for smart gas sensors. *J. Microelectromech. Syst.* 17(6): 1408-1417.

Baroncini M, Placidi P, Cardinali GC and Scorzoni A 2004 Thermal characterization of a microheater for micromachined gas sensors. *Sens. Actuators* A 115: 8-14.

Bose J-M, Guo Y, Sarihan V and Lee T 1998 Accelerated life testing for micro-chemical sensors. IEEE Trans. Reliab. 47: 135–141.

Briand D, Krauss A, van der Schoot B, Weimar U, Barsan N, Gopel W and de Rooij NF 2000 Design and fabrication of high-temperature micro-hotplates for drop-coated gas sensors. *Sens. Actuators B* 68: 223-233.

Briand D, Beaudoin F, Courbat J, de Rooij NF, Desplats R and Perdu P 2005 Failure analysis of micro-heating elements suspended on thin membranes. *Microelectron. Reliab*. 45: 1786-1789.

Briand D, Tomassone G-M and de Rooij NF 2003 Accelerated ageing of micro-hotplates for gas sensing applications. Proc. of IEEE sensors conference (Toronto, Canada): 1314-1317.

Briand D, Heimgartner S, Gretillat MA, Bart vdS and Rooij NFde 2002 Thermal optimization of micro-hotplates that have a silicon island. *J. Micromech. Microeng*. 12: 971-978.

Cardinali GC, Dori L, Fiorini M, Sayago I, Faglia G, Perego C, Sberveglieri G, Liberali V, Maloberti F and Tonetto DA 1997 Smart sensor system for carbon monoxide detection. *Anal. Integ. Circ. Sign. Process.* 14: 275-296.

Cossou B, Jacques S, Couégnat G, King SW, Li, L, Lanford WA, Bhattarai G, Paquette MM, Chollon G 2019 Synthesis and optimization of low-pressure chemical vapor deposition-silicon nitride coatings deposited from SiHCl3 and NH3. *Thin Solid Films* 681: 47-57

Courbat J, Briand D and de Rooij NF 2008 Reliability improvement of suspended platinum-based micro-heating elements. *Sens. Actuators A* 142: 284-291.

Deal BE and Grove AS 1965 General relationship for the thermal oxidation of silicon. J. Appl. Phys. 36: 3770

Faglia G, Comini E, Pardo M, Taroni A, Cardinali GC, Nicoletti S and Sberveglieri G 1999 Micromachined gas sensors for environmental pollutants. *Microsyst. Technol.* 6: 54-59.

Firebaugh SL, Jensen KF and Schmidt MA 1998 Investigation of high-temperature degradation of platinum thin films with an in situ resistance measurement apparatus. *J. Microelectromech. Syst.* 7: 128–135.

Fogarassy E, Slaoui A, Fuchs C and Regolini JL 1987 Rapid thermal oxidation of silicon monoxide. Appl. Phys. Lett. 51: 337–339

French PJ, Gennissen PTJ and Sarro PM 1997 New silicon micromachining techniques for Microsystems. *Sens. Actuators A* 62: 652-662.

Guidi V, Cardinali GC, Dori L, Faglia G, Ferroni M, Martinelli G, Nelli P and Sberveglieri G 1998 Thin-film gas sensor implemented on a low-power-consumption micromachined silicon structure. *Sens. Actuators* B 49: 88-92.

Kalinin IA, Roslyakov IV, Tsymbarenko DM, Bograchev DA, Krivetskiy VV and Napolskii KS 2021 Microhotplates based on Pt and Pt-Rh films: The impact of composition, structure, and thermal treatment on functional properties. *Sens. Actuators A* 317: 112457.

Konz W, Hildenbrand J, Bauersfeld M, Hartwig S, Lambrecht A, Lehmann V and Wollenstein J 2005 Micromachined IR-source with excellent black-body like behaviour. *Proc. SPIE* 5836: 540-548.

Li B, Zhou Q, Peng R, Liao Y and Zeng W 2021 Adsorption of SF6 decomposition gases (H2S, SO2, SOF2 and SO2F2) on Sc-doped MoS2 surface: A DFT study. *Appl. Surf. Sci.* 549: 149271.

Liu Q, Ding G, Wang Y, and Yao J 2018 Thermal performance of micro hotplates

with novel shapes based on single-layer SiO2 suspended film. *Micromachines* 9: 514.

Marciuš M, Ristic M, Ivanda M and Music S 2012 Formation and microstructure of nickel oxide films. *J. Alloys Compd*. 541(15): 238-243.

Mo Y, Okawa Y, Tajima M, Nakai T, Yoshiike N and Natukawa K 2001 Micro-machined gas sensor array on metal film micro-heater. *Sens. Actuators B* 79: 175-181.

Prasad M, Arya DS and Khanna VK 2015 Fabrication and reliability study of a double spiral platinum-based MEMS hotplate. *J. Micro/Nanolith*. MEMS MOEMS 14(2): 025003.

Puigcorbe J, Vogel D, Michel B, Vila A, Gracia I, Cane C and Morante JR 2003 Thermal and mechanical analysis of micromachined gas sensors. *J. Micromech. Microeng.* 13(5): 548-556.

Purohit S, Swarnalatha V, Pandey AK and and Pa P 2022 Wet anisotropic etching characteristics of Si{111} in NaOH-based solution for silicon bulk micromachining. *Micro Nano Syst. Lett.* 10:21

Rossi C, Briand D, Dumonteuil M, Camps T, Pham PQ and de Rooij NF 2006 Matrix of 10 × 10 addressed solid propellant microthrusters: review of the technologies. *Sens. Actuators A* 126: 241-252.

Samaeifar F, Hajghassem H, Afifi A and Abdollahi H 2015 Implementation of high-performance MEMS platinum micro-hotplate. Sens. Rev. 35(1): 116-124.

Sarro PM, Herwaarden AWv and vander Vlist W 1994 A silicon–silicon nitride membrane fabrication process for smart thermal sensors. *Sens. Actuators A* 41-42: 666-671.

Schössler T, Schön F, Lemier C and Urban G 2020 Reliability improvements of thin film platinum resistors on wafer-level and micro-hotplates at stress temperatures in the range of 140-290 °C. *Microelectron. Reliab.* 104: 113557.

Shwetha HR and Rudraswamy SB 2021 Design And fabrication of platinum-based mems microheater with integrated temperature sensor for the thermal analysis of greenhouse gases. *Nat. Volatiles Essent. Oils* 8(6): 3414-3424.

Simon I, Barsan N, Bauer M and Weimar U 2001 Micromachined metal oxide gas sensors: opportunities to improve sensor performance. *Sens. Actuators B* 73: 1-26.

Yan W, Xue N, Shi X, Liu J and Guo J 2008 Study on metal membrane temperature sensor and microheater for PCR chip. *Surf. Rev. Lett.* 15: 183.

Yuan Z, Yang F and Meng F 2022 Research progress on coating of sensitive materials for micro-hotplate gas sensor. *Micromachines* 13: 491.

Zhang K, Rossi C, Petrantoni M and Mauran N 2008 A nano initiator realized by integrating Al/CuO-based nanoenergetic materials with a Au/Pt/Cr microheater. *J. Microelectromech. Syst.* 17(4): 832-836.

Zhang KL, Chou SK and Ang SS 2007 Fabrication, modeling and testing of a thin film Au/Ti microheater. *Int. J. Thermal Sci.* 46(6): 580-588.

Zhou T and Zhang T 2021 Recent progress of nanostructured sensing materials from 0D to 3D: overview of structure-property-application relationship for gas sensors. *Small Methods* 5: 2100515.